JACS
JOURNAL OF THE AMERICAN CHEMICAL SOCIETY

COMMUNICATION

pubs.acs.org/JACS

Resting and Active States of the ERK2:HePTP Complex

Dana M. Francis,[†,∥] Bartosz Różycki,[‡,∥] Antoni Tortajada,[§] Gerhard Hummer,[‡] Wolfgang Peti,[†] and Rebecca Page*[,§]

[†]Department of Molecular Pharmacology, Physiology and Biotechnology, Brown University, Providence, Rhode Island 02912, United States

[‡]Laboratory of Chemical Physics, National Institute of Diabetes and Digestive and Kidney Diseases, National Institutes of Health, Bethesda, Maryland 20892, United States

[§]Department of Molecular Biology, Cell Biology and Biochemistry, Brown University, Providence, Rhode Island 02912, United States

Supporting Information

ABSTRACT: The MAP kinase ERK2 (ERK2, extracellular signal-regulated kinase 2) is regulated by numerous phosphatases that tightly control its activity. For example, the hematopoietic tyrosine phosphatase (HePTP) negatively regulates T cell activation in lymphocytes via ERK2 dephosphorylation. However, only very limited structural information is available for these biologically important complexes. Here, we use small-angle X-ray scattering combined with EROS ensemble refinement to characterize the structures of the resting and active states of ERK2:HePTP complexes. Our data show that the resting state ERK2:HePTP complex adopts a highly extended, dynamic conformation that becomes compact and ordered in the active state complex. This work experimentally demonstrates that these complexes undergo significant dynamic structural changes in solution and provides the first structural insight into an active state MAPK complex.

The mitogen-activated protein (MAP) kinase ERK2 (ERK2, extracellular signal-regulated kinase 2) is a ubiquitously expressed ser/thr kinase that is activated by extracellular stimuli and mediates a diverse set of cellular responses by phosphorylating a variety of protein substrates.[1] ERK2 activation is finely tuned in a cell-type specific and temporal manner by the concerted action of multiple regulatory proteins, including upstream kinases (MEK1/MEK2), scaffolding proteins (KSRs), MAPK phosphatases, and the kinase interaction motif (KIM) protein tyrosine phosphatases (KIM-PTPs).[2,3] Moreover, disruptions in ERK2 regulation are correlated with disease, such as Alzheimer's disease and cancer.[4,5] Consequently, ERK2 is an important drug target. Nevertheless, structural data of complete ERK2 regulatory complexes, which provides the necessary input for the identification of novel drug binding sites, are entirely missing.

ERK2 is activated by phosphorylation on a threonine (Thr183) and a tyrosine (Tyr185) residue in the ERK2 activation loop.[6,7] This phosphorylation is catalyzed by one of its two canonical upstream kinases MEK1 or MEK2. ERK2 is deactivated by the action of multiple phosphatases, including MAPK phosphatases, serine/threonine phosphatases, and tyrosine specific phosphatases.[8] Thus, while the kinase cascades that trigger MAP kinase activation seem stereotypic, phosphatases provide the guidance and fine-tuning that are critical for cell- and situation-specific responses.

KIM-PTPs form an important family of phosphatases that regulate ERK2 phosphorylation and cellular localization. The KIM-PTP family of proteins includes hematopoietic tyrosine phosphatase (HePTP; immune system specific[9]), striatum-enriched phosphatase (STEP; brain specific[10]), and STEP-like PTP (PTP-SL/PTPRR; brain specific[11]). Each KIM-PTP possesses a C-terminal phosphatase domain (PTP domain) and an N-terminal unstructured extension, which contains the 15 amino acid KIM (kinase interaction motif).[12] This motif has been identified in nearly every MAPK regulatory and substrate protein.[13,14] The KIM is characterized by a group of basic residues (K/R_{2-3}) and hydrophobic residues (Ø-x-Ø) that mediates the interaction with the KIM/D-motif binding groove of MAPKs.

The binding of KIM-PTPs to ERK2, via their KIMs, enables the activity of ERK2 to be regulated by both protein localization and dephosphorylation of its active site.[15] For example, HePTP, the only *p*Tyr-specific PTP known to dephosphorylate ERK2 in lymphocytes, is critical for modulating TCR activation through MAP kinase signaling. In resting T cells, HePTP associates via its KIM with the inactive unphosphorylated form of ERK2, retaining ERK2 in the cytosol (the ERK2:HePTP resting state complex). HePTP also associates via its KIM with the active, phosphorylated form of ERK2 and catalyzes the dephosphorylation of Tyr185, leading to the inactivation of ERK2 (the active state complex). In spite of the multitude of available ERK2 structures (inactive,[16,17] active,[18] MAPK:peptide complexes[19−23]), a detailed understanding of the structures and functions of the ERK2 complexes formed in the cell is missing. A major reason for the paucity of structural data is that these ERK2 complexes are dynamic and crystallization of large multiprotein kinase complexes has proven exceedingly difficult. Here we used small-angle X-ray scattering (SAXS) to gain a detailed understanding of how the ERK2 complexes that regulate the strength and duration of MAPK signaling interact in solution. These new solution structural models provide the necessary insights to understand the regulation of ERK2 at a molecular level.

We previously showed that HePTP is a monomer in solution that does not exhibit any signs of aggregation, allowing for the measurement of high quality SAXS data.[24] ERK2 is also a monomer in solution as determined using size exclusion chromatography (SEC; Superdex 75 26/60; GE Healthcare). A sharp

Received: August 9, 2011
Published: October 10, 2011

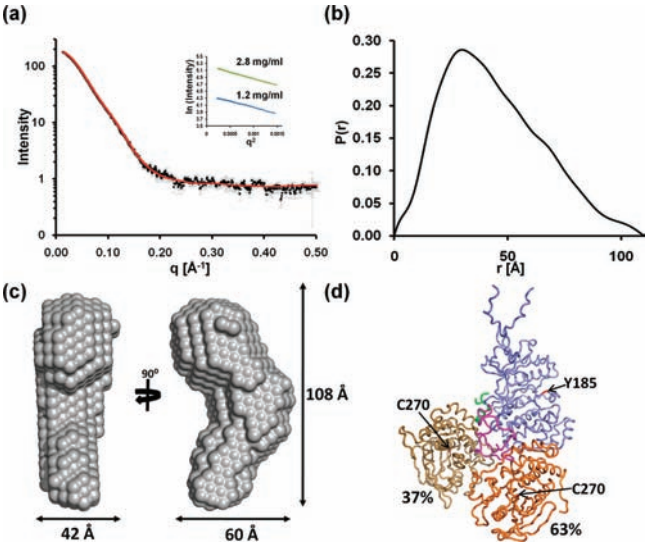

Figure 1. SAXS analysis of the ERK2:HePTP resting state complex. (a) Experimental SAXS data ($I(q)$ vs q) of the ERK2:HePTP resting state complex shown as black squares with error bars as gray lines. The theoretical scattering curve from the two-model ensemble is shown in red. *Inset,* Guinier plots, data recorded at 1.2 and 2.8 mg/mL. (b) The $P(r)$ function. (c) *Ab initio* molecular envelope generated by GASBOR, in two views rotated by 90°, with dimensions indicated. (d) Two-model ensemble, with the percentages that each model contributes to the scattering; ERK2 is blue, HePTP-KIM is green, HePTP-KIS is magenta, and two models of HePTP catalytic domain are in hues of orange. The locations of C270 (HePTP) and Y185 (ERK2) are indicated.

peak elutes at 174 mL corresponding to a molecular mass of ~42 kDa, exactly as expected for monomeric ERK2 (see Supporting Information (SI)). However, in contrast to HePTP and in spite of extensive measures to prevent any multimerization (i.e., ERK2 was purified by SEC within 14 h of SAXS data collection and the sample filtered using a 0.02 μm Whatman filter immediately prior to SAXS measurements), all data collected on apo-ERK2 contain the typical SAXS hallmark of aggregation, namely a rapid increase of the scattering intensity in the Guinier range. Thus, under the conditions tested, a fraction of ERK2 aggregates at the concentration needed for SAXS measurements at NSLS X9.

In sharp contrast to monomeric ERK2, ERK2:HePTP complexes (80 kDa), which form heterodimers in solution as tested by coelution using SEC (see SI), do not aggregate. As a result, SAXS measurements produced high-quality data for these complexes. The SAXS profile $I(q)$ and the corresponding pair distance distribution function $P(r)$ for the ERK2:HePTP resting state complex are shown in Figure 1a,b. Using the Guinier approximation of five independent SAXS samples, a radius of gyration (R_g) of 33.3 ± 0.7 Å was calculated for the ERK2:HePTP resting state complex (measurement statistics are reported in Table 1).[25] *Ab initio* determination of the molecular envelope also converged to an R_g of 34.2 Å and a maximum particle dimension of 110 Å (Figure 1c). These values for R_g are 6.9 and 8.0 Å larger than predicted for a globular protein with the same number of amino acids.[26] Collectively, these results demonstrate that, under resting conditions, the proteins adopt an extended head-to-head or head-to-tail conformation, with a rather limited interaction surface, similar to what has been observed for the p38:HePTP complex.[24] Clearly, this interaction does not entirely suppress

Table 1. Statistics for SAXS Analysis of the ERK2:HePTP Resting and Active State Complex

	Resting	Active
Guinier		
R_g (Å)	33.3 ± 0.7 (46 points)	30.3 ± 0.3 (55 points)
I_0/c	64.4 ± 2.0	47.0 ± 0.7
$P(r)$ function		
q-range (Å^{-1})	0.013−0.504	0.013−0.504
R_g (Å)	34.2	30.3
D_{max} (Å)	110	102.5
NSD[a]	1.25 ± 0.04	1.21 ± 0.03

[a] Averaged normalized spatial discrepancy.

flexibility, which helps explain why crystallization efforts have so far been unsuccessful.

In order to determine the relative orientation of ERK2 and HePTP in the resting state complex from the SAXS data, we used a recently developed computational procedure, the ensemble refinement of SAXS (EROS).[27] EROS proceeds in two steps: first, a coarse-grained model for protein binding is used to simulate the molecular assembly; second, the resulting ensemble of protein conformations is refined to improve the fit to the SAXS data. For the EROS simulations, an initial model of the ERK2:HePTP complex was generated using the crystal structures of the ERK2:HePTP KIM peptide complex (PDBID 2GPH)[23] and our previously determined HePTP catalytic domain (3D44; see SI).[28] The ERK2:HePTP KIM peptide and the HePTP catalytic domain were kept rigid. The HePTP kinase specificity sequence (KIS) linker (residues 31−56)[29] were treated as flexible based on the results of recent NMR spectroscopy experiments on the related p38:HePTP complex.[24] The conformational space occupied by these rigid bodies was thoroughly sampled by simulation to identify conformations that best fit the SAXS data. The best fit to the experimental data was obtained for an ensemble of two conformations, which fits the data with $\chi^2 = 1.26$ (Figure 1a, red line; Figure 1d). Both models are globally similar, with ERK2 and HePTP associating in an end-to-end manner with the HePTP catalytic domain localized below ERK2. They differ in the relative position of the catalytic domain, suggesting its position below ERK2 is dynamic. These motions are accommodated by changes in the flexible KIS linker connecting the HePTP KIM with the catalytic domain. Thus, under resting state conditions, HePTP and ERK2, analogous to HePTP and p38, form an extended complex in which the catalytic domain of HePTP is localized below ERK2 and distal from its activation loop.

An equivalent SAXS analysis was performed for the ERK2:HePTP active state complex. This complex represents a 'substrate trapping' complex (pTpY-ERK2:HePTP$_{STM}$, hereafter referred to as the ERK2:HePTP active state complex) in which the phosphorylated tyrosine of dually phosphorylated ERK2 (pTpY-ERK2) is bound at the active site of a catalytically inactive HePTP substrate trapping mutant (HePTP$_{STM}$, HePTP T106D/C270S) (see SI).[28] The Guinier approximation of five independent SAXS samples was used to calculate an $R_g = 30.3 \pm 0.3$ Å for the ERK2:HePTP active state complex (Figure 2a; Table 1).[25] Thus, in solution the R_g of the ERK2:HePTP active state complex is ~3.0 Å smaller than that of the ERK2:HePTP resting state complex. To analyze this difference in more detail, we determined the $P(r)$ function of the ERK2:HePTP active state complex.

dx.doi.org/10.1021/ja2075136 |J. Am. Chem. Soc. 2011, 133, 17138–17141

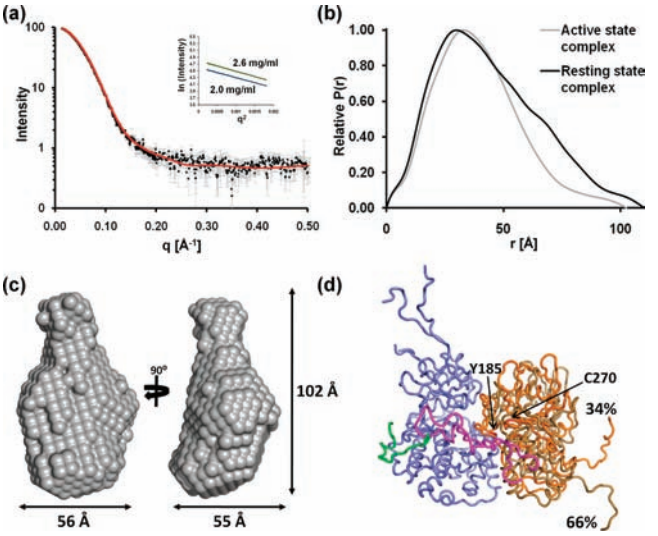

Figure 2. SAXS analysis of the ERK2:HePTP active state complex. (a) Experimental SAXS data ($I(q)$ vs q) of the ERK2:HePTP active state complex shown as black squares with error bars as gray lines. The theoretical scattering curve from the EROS refined model is shown in red. *Inset,* Guinier plots of data recorded at 2.0 and 2.6 mg/mL. (b) The $P(r)$ functions of the activated (gray) and resting (black) complexes. (c) *Ab initio* molecular envelope generated by GASBOR, in two views rotated by 90° with dimensions indicated. (d) Two-model ensemble, with the percentages that each model contributes to the scattering; colored as in Figure 1.

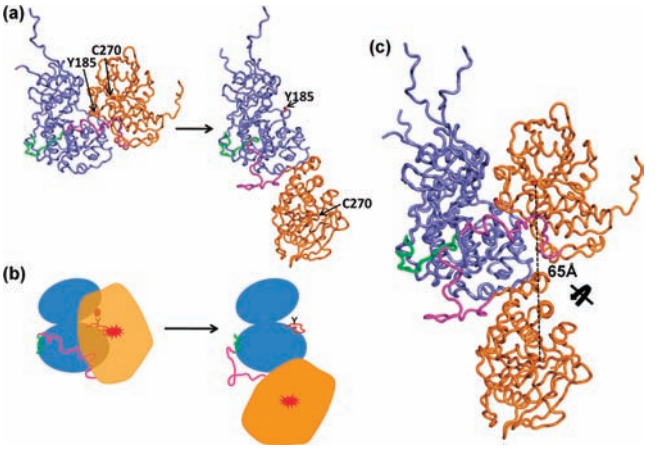

Figure 3. Active to resting transition. (a) Ribbon diagram and (b) cartoon representation of the active (left) and resting (right) states of the ERK2:HePTP complex; colored as in Figure 1. (c) Superposition of ERK2 active and resting state complexes. In the active state, the active site of HePTP is perfectly positioned to interact with the phosphorylated tyrosine on the ERK2 activation loop. Following dephosphorylation by HePTP, the HePTP catalytic domain rotates by nearly 180° and moves away from the ERK2 activation loop resulting in the extended resting state complex. The HePTP active site cysteine moves by ~65 Å between the active and resting state complexes.

A maximal length of only 102.5 Å was determined by analysis of the $P(r)$ function (Figure 2b), which was 7.5 Å shorter than that of the resting state. A comparison of the activated and resting state $P(r)$ functions in Figure 2b shows the clear differences between the two complexes. Finally, *ab initio* determination of the molecular envelope also converged on an R_g of 30.3 Å (Figure 2c). These analyses show that the ERK2:HePTP active state complex is significantly more compact than the resting state complex.

To further investigate the ERK2:HePTP active state complex in solution, we used EROS to determine the conformation of HePTP and ERK2 that optimally fits the experimental SAXS data.[27] In contrast to the ERK2:HePTP resting state complex, which has one point of contact between the two proteins (i.e., the HePTP KIM is bound to the ERK2 KIM docking groove), the ERK2:HePTP active state complex has two points of contact. In addition to the KIM interaction, the phosphorylated tyrosine of ERK2 is trapped at the active site of the HePTP. Using the crystal structure of activated ERK2 (2ERK)[18] in addition to those used to model the resting state complex, we generated an initial model for the ERK2:HePTP active state complex, in which the HePTP KIM was bound to the ERK2 KIM docking groove and the ERK2 pY185 was bound at the HePTP active site (see SI). In the simulations, two rigid bodies (ERK2, except for its activation loop, and the HePTP KIM peptide constitute rigid body 1, while pY185 of ERK2 and the HePTP catalytic domain constitute rigid body 2) were connected by three flexible linkers: (1) the HePTP KIS, connecting the HePTP KIM and catalytic domains; (2) ERK2 activation loop residues 172−184, the activation loop residues N-terminal to pY185; and (3) ERK2 activation loop residues 186−189, the activation loop residues C-terminal to pY185.

Similar to the computational analysis of the ERK2:HePTP resting state, the conformational space occupied by these rigid bodies and flexible linkers was thoroughly sampled by simulation to identify conformations that best fit the SAXS data. As for the resting state, the best fit to the active state experimental data was obtained for an ensemble of two conformations, with $\chi^2 = 1.17$ (Figure 2a, red line, Figure 2d). The two selected conformations are structurally highly similar, which suggests that the ERK2:HePTP complex is rather constrained in the active state. The ERK2:HePTP active state complex is more globular than that of the resting state complex. The HePTP catalytic domain is positioned next to the activation loop of ERK2, rather than below it, which is necessary for pY185 of ERK2 to bind the HePTP active site. This change in HePTP catalytic domain positioning is accommodated by changes in the conformation of the HePTP KIS and, to a lesser extent, changes in the conformation of the ERK2 activation loop.

MAP kinases and KIM-PTPs adopt multiple conformations to mediate subcellular localization (resting state), phosphorylation (MAP kinases phosphorylate KIM-PTPs), or dephosphorylation (KIM-PTPs dephosphorylate the pY residue of activated MAP kinases). Here, we show that resting and activated ERK2 are monomeric both alone and in complex with HePTP (see SI). These data contrast with previous work that suggest activated ERK2 self-associates to form homodimers both *in vitro*[18,30] and *in vivo*[31] but are consistent with more recent data from the Dalby group, which show that untagged activated ERK2 is monomeric under a variety of experimental conditions and when bound to the scaffolding protein PEA-15.[32]

Remarkably, when ERK2 is bound to HePTP, no dynamic aggregation is observed and the heterodimeric complexes give excellent scattering data for analysis of the complexes in solution. Using SAXS coupled with EROS refinement, we show that, under resting state conditions, the ERK2:HePTP complex adopts an elongated conformation in which the two proteins are tethered end-to-end via the HePTP KIM that is best described by a two-model ensemble. This suggests the position of the HePTP catalytic

domain below the ERK2 C-terminal domain is not fixed but instead dynamic. This is exactly what was observed for the p38:HePTP complex,[24] which also associates in an elongated end-to-end manner. Finally, a model based on cross-linking distances was recently proposed for the ERK2:PTP-SL resting state complex,[33] which predicted a more compact fold, similar to the activated ERK2:HePTP complex. Thus, the resting state p38:HePTP and ERK2:HePTP complexes differ from the predicted resting state ERK2:PTP-SL complex.[33] These differences suggest that the conformation of resting state MAPK:KIM-PTP complexes may be determined predominantly by the nature of the interacting KIM-PTP and not the MAPK.

In contrast to the ERK2:HePTP resting state, in which the two proteins associate in an end-to-end manner, the structure of the active state ERK2:HePTP complex reveals that the two proteins associate in a side-by-side manner, allowing the pY185 residue of the pTpY-ERK2 activation loop to bind the HePTP active site pocket in a mode identical to that observed for the HePTP:ERK2 peptide complex.[28] This is achieved by a nearly 180° rotation of the HePTP catalytic domain from below the C-terminal domain of ERK2 up toward the activation loop, which is located at the interface of the N- and C-terminal domains (Figure 3). This rotation is accommodated by a change in the conformation of the HePTP KIS (residues 31−56). As a consequence, the HePTP active site cysteine moves by ∼65 Å so that it is optimally positioned in the activated complex to dephosphorylate ERK2 residue pY185. In addition, because of the structural constraints on the conformation of the ERK2 activation loop (see SI), this rotation leads to a more extensive interaction between both the N- and C-terminal domains of ERK2 and HePTP than is observed in the resting state (Figure 3).

The ability to monitor these dynamic MAP kinase complexes in solution using SAXS coupled with EROS refinement has provided detailed models of their structures in the resting and active states. As only very limited protein:protein complex structural data for MAP kinases are available, this combined approach will be very valuable for the characterization of this critical class of proteins and their regulatory and substrate interactions.

■ ASSOCIATED CONTENT

Supporting Information. Experimental procedures, figures, and reference 21. This material is available free of charge via the Internet at http://pubs.acs.org.

■ AUTHOR INFORMATION

Corresponding Author
Rebecca_Page@brown.edu

Author Contributions
‖These authors contributed equally.

■ ACKNOWLEDGMENT

The authors thank Drs. Lin Yang and Marc Allaire (NSLS, X9) for their support. The project was supported by Grant RSG-08-067-01-LIB from the American Cancer Society to R.P. B.R. was supported by a Marie Curie International Outgoing Fellowship within the 7th European Community Framework Program. B.R. and G.H. were supported by the Intramural Research Program of the National Institute of Diabetes and Digestive and Kidney Diseases, NIH. Use of the NSLS was supported by the U.S. DOE, Office of Science under Contract No. DE-AC02-98CH10886. Simulations were performed on the Biowulf computing cluster at NIH.

■ REFERENCES

(1) Raman, M.; Chen, W.; Cobb, M. H. *Oncogene* **2007**, *26*, 3100.
(2) Imajo, M.; Tsuchiya, Y.; Nishida, E. *IUBMB Life* **2006**, *58*, 312.
(3) Brown, M. D.; Sacks, D. B. *Cell Signal* **2009**, *21*, 462.
(4) Kim, E. K.; Choi, E. J. *Biochim. Biophys. Acta* **2010**, *1802*, 396.
(5) Snyder, E. M.; Nong, Y.; Almeida, C. G.; Paul, S.; Moran, T.; Choi, E. Y.; Nairn, A. C.; Salter, M. W.; Lombroso, P. J.; Gouras, G. K.; Greengard, P. *Nat. Neurosci.* **2005**, *8*, 1051.
(6) Robbins, D. J.; Zhen, E.; Owaki, H.; Vanderbilt, C. A.; Ebert, D.; Geppert, T. D.; Cobb, M. H. *J. Biol. Chem.* **1993**, *268*, 5097.
(7) Seger, R.; Ahn, N. G.; Boulton, T. G.; Yancopoulos, G. D.; Panayotatos, N.; Radziejewska, E.; Ericsson, L.; Bratlien, R. L.; Cobb, M. H.; Krebs, E. G. *Proc. Natl. Acad. Sci. U.S.A.* **1991**, *88*, 6142.
(8) Alonso, A.; Sasin, J.; Bottini, N.; Friedberg, I.; Osterman, A.; Godzik, A.; Hunter, T.; Dixon, J.; Mustelin, T. *Cell* **2004**, *117*, 699.
(9) Zanke, B.; Suzuki, H.; Kishihara, K.; Mizzen, L.; Minden, M.; Pawson, A.; Mak, T. W. *Eur. J. Immunol.* **1992**, *22*, 235.
(10) Lombroso, P. J.; Murdoch, G.; Lerner, M. *Proc. Natl. Acad. Sci. U.S.A.* **1991**, *88*, 7242.
(11) Hendriks, W.; Schepens, J.; Brugman, C.; Zeeuwen, P.; Wieringa, B. *Biochem. J.* **1995**, *305* (Pt 2), 499.
(12) Pulido, R.; Zuniga, A.; Ullrich, A. *EMBO J.* **1998**, *17*, 7337.
(13) Bardwell, A. J.; Frankson, E.; Bardwell, L. *J. Biol. Chem.* **2009**, *284*, 13165.
(14) Bardwell, L. *Biochem. Soc. Trans.* **2006**, *34*, 837.
(15) Saxena, M.; Williams, S.; Brockdorff, J.; Gilman, J.; Mustelin, T. *J. Biol. Chem.* **1999**, *274*, 11693.
(16) Wang, Z.; Harkins, P. C.; Ulevitch, R. J.; Han, J.; Cobb, M. H.; Goldsmith, E. J. *Proc. Natl. Acad. Sci. U.S.A.* **1997**, *94*, 2327.
(17) Zhang, F.; Strand, A.; Robbins, D.; Cobb, M. H.; Goldsmith, E. J. *Nature* **1994**, *367*, 704.
(18) Canagarajah, B. J.; Khokhlatchev, A.; Cobb, M. H.; Goldsmith, E. J. *Cell* **1997**, *90*, 859.
(19) Bhattacharyya, R. P.; Remenyi, A.; Good, M. C.; Bashor, C. J.; Falick, A. M.; Lim, W. A. *Science* **2006**, *311*, 822.
(20) Chang, C. I.; Xu, B. E.; Akella, R.; Cobb, M. H.; Goldsmith, E. J. *Mol. Cell* **2002**, *9*, 1241.
(21) Heo, Y. S.; et al. *EMBO J.* **2004**, *23*, 2185.
(22) Liu, S.; Sun, J. P.; Zhou, B.; Zhang, Z. Y. *Proc. Natl. Acad. Sci. U.S.A.* **2006**, *103*, 5326.
(23) Zhou, T.; Sun, L.; Humphreys, J.; Goldsmith, E. J. *Structure* **2006**, *14*, 1011.
(24) Francis, D. M.; Różycki, B.; Koveal, D.; Hummer, G.; Page, R.; Peti, W. *Nat. Chem. Biol.* **2011**, in press.
(25) Guinier, A. *Ann. Phys.* **1939**, *12*, 161.
(26) Gong, H.; Freed, K. F. *Biophys. J.* **2010**, *98*, 470.
(27) Rozycki, B.; Kim, Y. C.; Hummer, G. *Structure* **2011**, *19*, 109.
(28) Critton, D. A.; Tortajada, A.; Stetson, G.; Peti, W.; Page, R. *Biochemistry* **2008**, *47*, 13336.
(29) Munoz, J. J.; Tarrega, C.; Blanco-Aparicio, C.; Pulido, R. *Biochem. J.* **2003**, *372*, 193.
(30) Wilsbacher, J. L.; Juang, Y. C.; Khokhlatchev, A. V.; Gallagher, E.; Binns, D.; Goldsmith, E. J.; Cobb, M. H. *Biochemistry* **2006**, *45*, 13175.
(31) Casar, B.; Pinto, A.; Crespo, P. *Mol. Cell* **2008**, *31*, 708.
(32) Kaoud, T. S.; Devkota, A. K.; Harris, R.; Rana, M. S.; Abramczyk, O.; Warthaka, M.; Lee, S.; Girvin, M. E.; Riggs, A. F.; Dalby, K. N. *Biochemistry* **2011**, *50*, 4568.
(33) Balasu, M. C.; Spiridon, L. N.; Miron, S.; Craescu, C. T.; Scheidig, A. J.; Petrescu, A. J.; Szedlacsek, S. E. *PLoS One* **2009**, *4*, e5432.